AIAA JOURNAL
Vol. 38, No. 2, February 2000

Adaptive Control of Shape Memory Alloy Actuators for Underwater Biomimetic Applications

G. Webb,* L. Wilson,† D. Lagoudas,‡ and O. Rediniotis§
Texas A&M University, College Station, Texas 77843-3141

In actuator technology active or smart materials have opened up new horizons in terms of actuation simplicity, compactness, and miniaturization potential. One such material is the nickel-titanium shape memory alloy (NiTi SMA), which is gaining widespread use in a variety of applications. The numerous advantages of SMA over traditional actuators are of particular interest in the area of underwater vehicle design, particularly the development of highly maneuverable vehicles of a design based on the swimming techniques and anatomic structure of fish. An SMA actuation cycle consists of heating/cooling half-cycles, currently imposing a limit on the frequency of actuation to well below 1 Hz in air because of slow cooling. The aquatic environment of underwater vehicles lends itself to cooling schemes that use the excellent heat-transfer properties of water, thus enabling much higher actuation frequencies. A controller for SMA actuators must account not only for large hysteretic nonlinearities between actuator output (strain or displacement) and input (temperature), but also the thermal control for resistive heating via an applied current. The control of SMA in water presents a problem not encountered when actuating in air: accurate temperature feedback for the SMA is very difficult in water. We overcome this problem by using a simplified thermal model to estimate the temperature of the wire in conjunction with an adaptive hysteresis model, which relates the actuator output to the estimated temperature. Experimental results are provided, showing that this method for control of an SMA wire works equally well both in air and in water, with only rough estimates (easily obtained) of the thermal parameters. Successful tracking of reference displacement signals with frequencies up to 2 Hz and relatively large amplitudes have been demonstrated experimentally.

I. Introduction

IN aerodynamics and hydrodynamics birds and fish have inspired and guided the development of aircraft and underwater vehicles. These manmade machines seem so primitive compared to their natural counterparts in terms of intelligence, efficiency, agility, adaptability, and functional complexity. These and other similar observations and issues that have been addressed by the scientific community have triggered the formulation of the science of biomimetics and have inspired new approaches to old problems. In the area of underwater vehicle design, the development of highly maneuverable vehicles is presently of interest, with their design being based on the swimming techniques and anatomic structure of fish; primarily the undulatory body motions, the highly controllable fins, and the large aspect ratio lunate tail. The tailoring and implementation of the accumulated knowledge into biomimetic vehicles is a task of multidisciplinary nature with two of the dominant fields being actuation and hydrodynamic control.

In actuator technology active or smart materials have opened up new horizons in terms of actuation simplicity, compactness, and miniaturization potential. Shape memory alloys (SMA) are such materials that develop strains or, more applicably, displacements when exposed to temperature changes. SMAs undergo a change in crystal structure from a parent cubic austenitic (A) phase to a number of martensitic (M) variants either upon cooling or application of stress.[1] The reverse phase change occurs, although with significant hysteresis, upon increasing the temperature and/or removal of stress. These phase changes, triggered by thermomechanical loading, are accompanied by significant deformations and when suitably constrained, produce large actuation forces (about three orders of magnitude higher as compared to piezoceramics). This effect is most significant in the Nitinol (NiTi) SMAs, which have been used as force and displacement actuators in a variety of applications.[2–4]

The present work is motivated by the effort to develop biomimetic underwater vehicles that share the agility, hydrodynamic efficiency, and stealth of aquatic animals. Several biomimetic principles are incorporated in the conceptual design shown in Fig. 1. In this design SMA actuators function as muscles and constitute the mechanical equivalent of the fish myotome. Either side of an individual actuator, in the longitudinal direction, is attached to the skeletal structure of the vehicle. This spined structure presented in Fig. 1 illustrates how SMA actuation (in the chordwise direction) causes body-shape changes, by rotating the skeletal vertebra. The dashed and solid lines representing the actuators in the schematic distinguish between the actuated and the relaxed SMAs, respectively.

For wire SMA actuators a convenient actuation means for the martensite-to-austenite (M to A) transformation is resistive heating of the SMA via the supply of an electrical current through it. The reverse austenite-to-martensite (A to M) transformation is achieved via cooling. Heat-removal mechanisms are inherently slower than electrical heat addition. Therefore, in a heating-cooling cycle necessary to complete a full SMA transformation/actuation cycle (M to A and then A to M), the cooling process usually limits the rapidity of the cycle, i.e., the maximum attainable frequency response. The aquatic environment of the vehicle lends itself to cooling schemes that use the excellent heat-transfer properties of water. The cooling approach explored in the present work involves forced water convection over the SMA. Whereas pure water is electrically insulative, we acknowledge the fact that the water used in laboratory experiments will contain impurities. However, the resistance of the water is many orders of magnitude greater than that of the SMA wire, and nearly all of the current will take the path of least resistance through the SMA. Experiments with stagnant air, forced-air convection, and forced-water convection show a logical progression of increased cooling rates requiring larger currents to achieve identical temperature changes. In future work we will employ electrically insulative, thermally conductive fluids (such as glycol) as the cooling agent.

In controlling an SMA, there are generally two methods of dealing with the hysteresis between the input (e.g., temperature or stress) and the output (e.g., strain, displacement, or force): 1) Open loop compensation, where we identify a phenomenological model that maps input to output and then invert the model to remove the nonlinearity, and 2) closed-loop feedback, where we use the output error (difference between the measured output and the desired output)

Received 9 November 1998; revision received 1 July 1999; accepted for publication 9 July 1999.

*Research Associate, Department of Aerospace Engineering.
†Graduate Assistant, Department of Aerospace Engineering.
‡Professor, Department of Aerospace Engineering.
§Assistant Professor, Department of Aerospace Engineering.

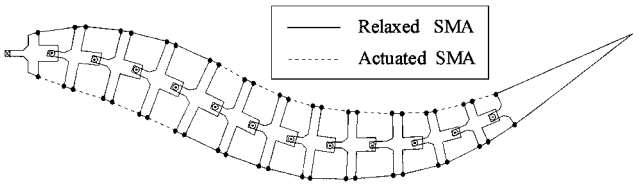

Fig. 1 Conceptual design of SMA-actuated underwater vehicle.

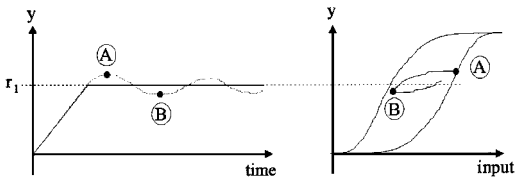

Fig. 2 Illustration of hysteresis phenomenon.

to calculate the heat input to the SMA. Open-loop compensation has the advantage of accounting for input history in determining the control and can usually be easily identified solely from input-output measurements. If the hysteresis model can be accurately identified, then the inverse model will provide the necessary input signal to track a desired output. The main disadvantage of this approach is that feedback is not incorporated into the controller to account for tracking error caused by noise, disturbances, and/or an inexact model. Conversely, the closed-loop feedback approach incorporates the tracking error directly into the control algorithm. For slowly varying reference signals, and with properly tuned gains, feedback strategies such as proportional-integral (PI) control can provide adequate performance. However, feedback control does not account for the input history, which dictates whether a small change in input will result in either a large or small change in output. An example of this phenomena is provided in Fig. 2. Here a PI controller with adequate gains should be able to track the ramp trajectory up to $y = r_1$. However, if there is even a slight overshoot (pt. A), a large decrease in the input is required to lower y back to r_1. Then, for even a small undershoot (pt. B) a large increase in the input is required to increase y only a small distance back to r_1. It can be very difficult to account for this behavior using only a feedback approach to control of SMA actuators, and oscillatory motions about the reference trajectory often occur. Examples of open-loop compensation approaches can be found in Refs. 5 and 6 and for closed-loop feedback approaches in Refs. 7 and 8.

Resistive heating introduces one of the main difficulties in hysteresis compensation methods for SMA wires, in that the output is hysteretically dependent upon the temperature history—not the electrical current input to the wire. There are many unknowns with the thermal actuation of SMA wires, such as the specific material properties as well as many variables that change with the surrounding environment. For example, ambient temperature, the surrounding medium, and external loading all have a profound influence on the response of an SMA wire. Actuation in water only magnifies the effect of the surrounding medium, where small changes in the water flow parameters can significantly affect the convection of heat from the SMA. In addition, heat transfer from the SMA to the water can cause variations in the local water temperature. Another difficulty imposed by underwater actuation is that the accurate temperature measurements of the SMA cannot be achieved via thermocouples. A thermocouple is attached to the SMA wire with a small ball of thermal paste that electrically, but not thermally, insulates the thermocouple bead from the wire. The thermocouple then measures the temperature of the thermal paste. Because of the high convectivity of the water, the thermal paste dissipates the heat from the wire much faster than in air, and the resulting temperature is not indicative of the temperature of the SMA. Even in still air, accurate SMA wire temperature measurements are difficult to obtain. An alternative to temperature measurements is to measure the resistivity of the wire. However, the resistivity is an output quantity for the SMA hysteresis: it is an indicator of the phase transformation as a function of temperature and therefore cannot be used as input to a hysteresis model. To alleviate the problem of direct temperature measurements of the SMA wire, we implement an observer based on a simplified thermal model of the SMA wire that requires only rough estimates of the thermal parameters.

The control approach in this work combines the advantages of both methods, implementing an adaptive hysteresis model for feedback compensation. This method has been studied numerically and experimentally for the control of SMA wire actuators.[9,10] In feedback compensation the tracking error is not directly used in the control law. Rather, it is used to update (identify on-line) the hysteresis model to account for discrepancies between the model and the actual input-output relationship. The inverse maps a desired reference trajectory into a temperature signal. When temperature can be measured, an adaptive thermal model then commands a current to control the temperature of the SMA to follow the desired temperature. For the case of underwater actuation, integration of a simplified thermal model, based only on rough estimates of the thermal parameters, is used in place of actual temperature measurements. Section II describes the prototype experiment for underwater actuation of a single SMA wire. Section III details the control methodology involving the adaptive hysteresis model and the thermal model for temperature estimation and control of the heating current. In Section IV we provide experimental results for tracking a variety of reference signals, including step displacement and sinusoidal signals of frequencies up to 2 Hz. The experiments are conducted both in air and in water to show the robustness of the control methodology for surrounding media with different thermal properties.

II. Experimental Setup

The purpose of the test stand, depicted in Fig. 3, is threefold: 1) provide power to the wire, 2) support the SMA wire in an unobstructed flowfield, and 3) provide a means to measure the actuation displacement of the wire. The C shape of the test stand allows the stand to support the SMA wire without disturbing the upstream flow around the wire. The SMA wire is connected to power leads by brass connectors, one on each end, where the bottom attachment provides structural support for the SMA actuator. The free end (top) of the wire is attached to the lever arm by a kevlar string so that wire lengths of 1–14 in. (1–34.6 cm) can be accommodated in the frame. A spring attached to the opposite end of the lever arm both holds the SMA wire in tension and provides a restoring force for the SMA. The spring was used instead of a constant weight (mass) because the inertial forces created by that mass at higher frequencies caused bouncing of the SMA wire, which resulted in compressive forces on the SMA wire. The lever arm magnifies the SMA displacement by a factor of 4, which is then measured using a Celesco string-potentiometer with a 30-in. (106-cm) displacement capacity.

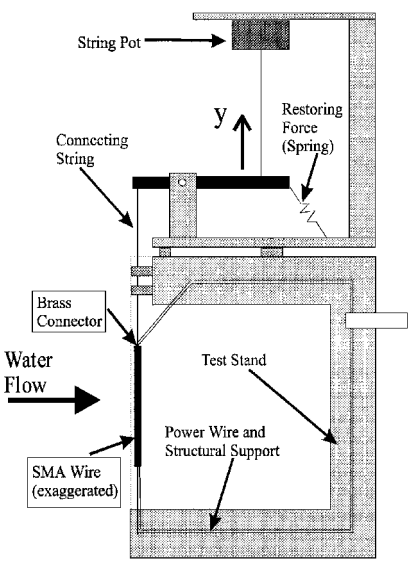

Fig. 3 Test stand.

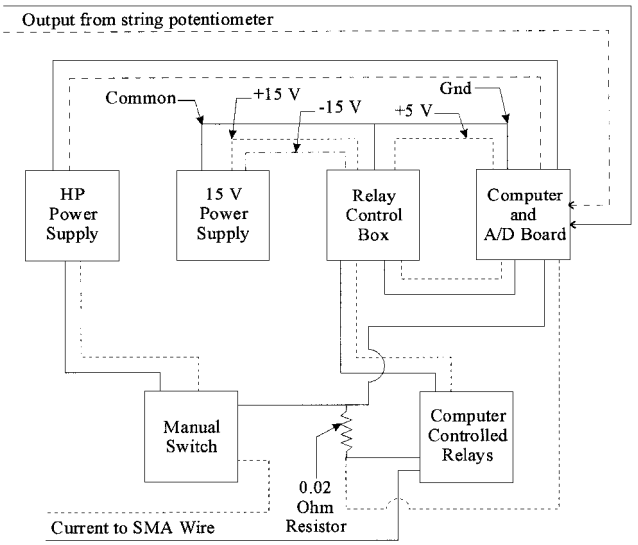

Fig. 4 Control circuit diagram.

The resolution of the string-potentiometer is 0.0008 in. (0.00263 cm). There are three components to the displacement uncertainty: the string-potentiometer voltage drift, noise in the lab, and string-potentiometer calibration error. The voltage drift and calibration error are on the order of ±3 mV, whereas the noise is ±0.3 mV. The total worst-case uncertainty is 0.010 in. (0.0254 cm). The average wire used in the test frame is 12 in. (30.5 cm) long, so at 2% strain the uncertainty in displacement would be 4.17% if the string-potentiometer displaces equally with the wire. When the string-potentiometer deflection is multiplied by four, the uncertainty is reduced by the same number to 1.04% of the wire's displacement, which is a much more acceptable error.

The test section of the water tunnel has a cross section of 2×3 ft (0.61×0.91 m). The tunnel is capable of speeds up to 0.9 m/s in the test section; however, the maximum water velocity used for the experiments in this work was 0.415 m/s. The components of the control circuit, depicted in Fig. 4, are a 1200-W Hewlett Packard 6268B power supply (HP power supply), relay control box, National Instrument's (NI) AT-MIO-16XE-50 A/D board installed in a Pentium 133 PC, two 16 A, 250vac relays in parallel, 12vdc actuated, and a 0.02 Ω 50-W resistor. The string-pot output voltage is read using a differential channel on the NI board and converted to displacement, labeled y in Fig. 3, providing the feedback measurements for the controller. The controller commands a specific current value. This request is converted to an analog signal, which controls the HP power supply. The HP power supply has an upper limit of 30 A, with a rise time of 0.054 s from 0 to 20 A. The voltage drop across the 0.02 Ω resistor is sampled by the NI board and yields a measurement of the actual current through the circuit for assurance that the power supply outputs the commanded current.

To address the issue of electrical current lost to the water, compare the resistance of the SMA wire used in the experiment with the resistance of the water: $R_{\text{wire}} \approx 2\,\Omega$ and $R_{\text{water}} \approx 1.5 \times 10^5\,\Omega$. Under the assumption that these two resistors are in parallel with 20 A from the power supply, only 0.13 mA is lost to the water. For another comparison, for 1% of the current to be lost to the water, the equivalent resistance of the water would need to be on the order of 100 Ω.

III. Adaptive Hysteresis Model with Temperature Estimation

When actuating an SMA wire by resistive heating, the input to the wire that can be directly commanded is the current. Our model for the SMA wire must then relate current to displacement. When the wire temperature can be measured, we can use a hysteresis model that maps a desired displacement into temperature in a series with a thermal control model that maps temperature into current. This method has been implemented successfully in laboratory experiments using an adaptive hysteresis model and an adaptive thermal model.[5,9,10] For the underwater applications of interest in this paper, temperature measurements would be difficult to obtain, and we must therefore alter the control strategy. One approach might be to relate the SMA displacement output directly with the current using a hysteresis model. However, the displacement vs current relationship is highly current-rate dependent and nonmonotonic, the former making it unsuitable for adaptive learning and the latter violating the basic laws for the hysteresis model.[9,11] We propose that even though the temperature of the wire cannot be measured and used as the input to the hysteresis model, it can be estimated using a simplified thermal model. This temperature estimate will serve to reduce/eliminate any rate dependence in the hysteresis model. This section discusses 1) the adaptive hysteresis model used to map temperature into displacement and to transform a reference displacement signal into a temperature signal via the inverse, 2) a simplified thermal model and the design of a control law to command a current signal for temperature tracking, 3) a calibration procedure to calculate rough estimates of the thermal parameters, and 4) the control algorithm that combines the adaptive hysteresis compensation, the temperature estimation, and the thermal control law.

A. Adaptive Hysteresis Model

The parameterized Krasnoselskii and Pokrovskii (KP) model, developed in Ref. 9, represents the hysteretic dependence of the SMA wire output on the temperature. The KP model is founded on the principle first introduced by Preisach,[12,13] where the output is an infinite sum of weighted simple hysteresis operators, or kernels. Krasnoselskii and Pokrovskii[14] developed a continuous version of the Preisach kernel, which allowed for finite-dimensional approximations of the infinite-dimensional model. Banks et al.[15,16] studied the mathematical properties of the infinite-dimensional KP model and proved the well-posedness for the inverse problem of identification of a finite-dimensional approximation. Webb[9] studied the finite-dimensional, parameterized version of the KP model for adaptive identification and compensation for control of hysteretic actuators. Webb et al.[10] provided experimental results for control of an SMA wire actuator using the adaptive KP model along with an adaptive thermal model to control the current input to the wire. Although only a summary of the parameterized KP model is given in this paper, the interested reader is directed to the preceding references for an in-depth background.

1. *Parameterized KP Model*

The parameterized KP model for use in adaptive control is developed[9,10] to solve the following problem: Given a hysteretic input-output relationship [e.g., displacement as a function of temperature, or $y = H(T)$], define a model that 1) is linear in the parameters $\theta = \{\theta_i\}^T$, $i = 1, \ldots, N$; 2) can be represented in the vector form

$$H(T) = \theta^T \boldsymbol{F}(T), \qquad \boldsymbol{F}(T) = \{f_i(T)\}^T, \qquad i = 1, \ldots, N \quad (1)$$

where $f_i(T)$ are independent functions of the temperature, and 3) has a mathematical structure well-suited for representation of the hysteresis. The form of Eq. (1) is essential for the application of gradient adaptive methods, which are well-documented in the literature (e.g., Ref. 17) and simple to implement.

For the model to represent the hysteresis, the functions of input must have the capability to account for the preceding input history in determining the output. The Preisach model concept, a summation of weighted hysteresis operators, provides the structure for such a model. However, the mathematical properties of the Preisach model are only well-defined for an infinite summation of Preisach operators.[15,16] For practical applications we require a model that is well-defined in finite dimensions, for which a class of operators known as KP operators have been shown to be well suited.[16] The actions of the Preisach and KP operators are depicted in Fig. 5. The Preisach operator can only exist at two states, +1 and −1, with instantaneous jumps between them. In contrast, the KP operator can exist at any value in the closed interval [−1, +1], with a continuous transformation between the two states.

Referring to Fig. 5b, the defining elements for a KP operator are as follows:

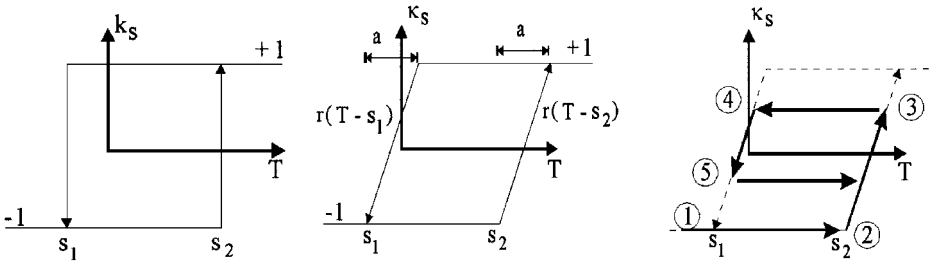

a) Preisach (k_s) **b) KP (κ_s)**

Fig. 5 Operators.

1) s_1, s_2 are the values of input (e.g., temperature) that determine the width of hysteresis.

2) $r(x)$ is the ridge function, which forms the left and right bounding curves for the hysteresis.

3) a is the rise interval of input over which the operator linearly evolves between the values of -1 and $+1$.

With the preceding notation a KP operator is written as κ_s, where $s = (s_1, s_2)$. The ridge function $r(x)$ is given by

$$r(x) = \begin{cases} -1, & x < 0 \\ -1 + 2\frac{x}{a}, & 0 \le x \le a \\ 1, & x > a \end{cases} \tag{2}$$

The following example illustrates the basic function of the KP operator. Consider the operator shown in Fig. 5b by the dashed line and the input-output relationship for some input history represented by the solid line.

Location 1: T is less than s_1 and $\kappa_s(T)$ is equal to -1. $\dot{T} > 0$.

Location 2: At this point $T = s_2$, and $\kappa_s(T)$ will begin to follow the right bounding curve $r(T - s_2)$.

Location 3: When $s_2 < T < s_2 + a$, $\dot{T}$ switches sign, and T begins to decrease. The output of the operator is recorded using a memory variable $\xi = \kappa_s(T)$. As T decreases, $\kappa_s(T)$ will remain at a value of ξ until $r(T - s_1) < \xi$.

Location 4: When $r(T - s_1) < \xi$, the output will follow the left bounding curve as T decreases.

Location 5: While $T > s_1$, the input switches from decreasing to increasing. The variable ξ is then updated with the new output value, and $\kappa_s(T)$ will remain at a value of ξ until $r(T - s_2) > \xi$.

The mathematical representation that describes the action of the KP kernel is given by

$$\kappa_s(T, \xi_s) = \begin{cases} \max\{\xi_s, r(T - s_2)\} & \text{if} \quad \dot{T} \ge 0 \\ \min\{\xi_s, r(T - s_1)\} & \text{if} \quad \dot{T} \le 0 \\ (\kappa_s)_{\text{previous}} & \text{if} \quad \dot{T} = 0 \end{cases} \tag{3}$$

where the memory term for a specific operator ξ_s is updated whenever $\dot{T}$ switches sign.

The parameterized KP model is formed from the summation of a finite number of weighted KP operators over a finite region of input, dictated by the interval of input over which hysteresis occurs, i.e., $[T_{\min}, T_{\max}]$. The input interval is discretized into K evenly spaced points. Because there are two values of input defining a KP operator s_1 and s_2, we require two axes (the s_1 axis and s_2 axis) to represent decreasing and increasing input, respectively. Close inspection of the operator in Fig. 5b reveals that an operator with switching values $(s_1, s_2) = (T_1, T_2)$ is simply the reverse of an operator with $(s_1, s_2) = (T_2, T_1)$. The conventional approach[13,16] is to choose the set of operators defined by $s_2 \ge s_1$. Hence, in the s_1-s_2 plane KP operators are defined for $s \in S$, where S is the space defined by

$$S = \{(s_1, s_2): s_2 \in [T_{\min}, T_{\max}],\ s_2 \ge s_1\} \tag{4}$$

forming the triangle shown in Fig. 6.

For the parameterized KP model there are a finite number of operators that represent the space S, given by $N = K(K + 1)/2$.

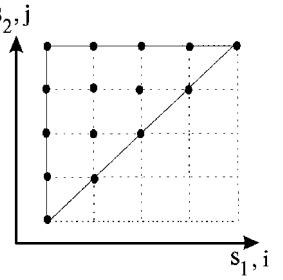

Fig. 6 *S*-plane grid.

Each grid point in Fig. 6 represents a KP operator. By creating (i, j) indices, an individual operator can be denoted by $\kappa_{s_{ij}}$, where

$$s_{ij} = (s_{1i}, s_{2j}), \qquad s_{1i} = T_{\min} + (i - 1)\Delta T$$

$$s_{2j} = T_{\min} + (j - 1)\Delta T, \qquad \Delta T = \frac{T_{\max} - T_{\min}}{K - 1} \tag{5}$$

The one property left to be defined is the rise interval a. From previous numerical studies[9] a good choice is to set $a = \Delta T$. Using the grid-point indices of (i, j), the parameterized KP hysteresis model can now be defined in the required vector form:

$$H(T) = \theta^T \boldsymbol{F}(T), \qquad \theta = \{\theta_{1,1}, \theta_{1,2}, \ldots, \theta_{1,K}, \theta_{2,2}, \ldots, \theta_{K,K}\}^T$$

$$\boldsymbol{F}(T) = \{\kappa_{s_{1,1}}, \kappa_{s_{1,2}}, \ldots, \kappa_{s_{1,K}}, \kappa_{s_{2,2}}, \ldots, \kappa_{s_{K,K}}\}^T \tag{6}$$

2. Gradient Adaptive Law

The gradient adaptive law is designed for functions that can be represented linearly in parameters in vector form, or $y = \theta^T F$. For application to the parameterized KP model, θ is a vector of weighting parameters, and $\boldsymbol{F}(T)$ is a vector of memory operators in T. Specifically, let θ represent the exact hysteresis parameters and $\hat{\theta}$ represent the parameter estimates:

$$y = H(T) = \theta^T \boldsymbol{F}(T), \qquad \hat{y} = \hat{H}(T) = \hat{\theta}^T \boldsymbol{F}(T) \tag{7}$$

The error between the two models is simply $e = y - \hat{y} = (\theta^T - \hat{\theta}^T)\boldsymbol{F}(T)$. To ensure signal boundedness, create the normalized estimation error

$$\varepsilon = (T - \hat{T})/m^2 = \tilde{\theta}^T \boldsymbol{F}(T)/m^2 \tag{8}$$

where $\tilde{\theta} = \theta - \hat{\theta}$ and m^2 is the normalizing signal:

$$m^2 = 1 + n_s, \qquad n_s = \boldsymbol{F}(T)^T \boldsymbol{F}(T) \tag{9}$$

designed such that m^2 is strictly greater than zero. Consider the quadratic cost function given by Eq. (10):

$$J(\hat{\theta}) = \frac{\varepsilon^2 m^2}{2} = \frac{[y - \hat{\theta}^T \boldsymbol{F}(T)]^2}{2m^2} \tag{10}$$

Then the minimizing trajectory for the cost function is given by the gradient of $J(\hat{\theta})$ as

$$\dot{\hat{\theta}} = -\Gamma \nabla J(\hat{\theta}) \tag{11}$$

where $\Gamma = \Gamma^T > 0$ is a scaling matrix of adaptive gains. The gradient of $J(\hat{\theta})$ is given as

$$\nabla J(\hat{\theta}) = -\{[y - \hat{\theta}^T \boldsymbol{F}(T)]\boldsymbol{F}(T)\}/m^2 = -\varepsilon \boldsymbol{F}(T) \tag{12}$$

resulting in the adaptive update law

$$\dot{\hat{\theta}} = \Gamma \varepsilon \boldsymbol{F}(T) \tag{13}$$

To ensure that the parameter estimates remain bounded in some set Q, derived from a priori knowledge of the properties of θ, we use a parameter projection term. By defining Q as

$$Q = \{\hat{\theta} \in \mathbb{R}^n : p(\hat{\theta}) \leq 0\} \tag{14}$$

where $p(\hat{\theta})$ is a vector of constraint equations on $\hat{\theta}$. The adaptive update law of Eq. (13) becomes

$$\dot{\hat{\theta}} = \begin{cases} \Gamma \varepsilon \boldsymbol{F}(T) & \text{if} \quad \hat{\theta} \in \text{interior}(Q) \quad \text{or} \\ & \hat{\theta} \in \text{boundary}(Q) \quad \text{and} \\ & [\Gamma \varepsilon \boldsymbol{F}(T)]^T \nabla p \leq 0 \\ \Gamma \varepsilon \boldsymbol{F}(T) - \Gamma \dfrac{\nabla p \nabla p^T}{\nabla p^T \Gamma \nabla p} \Gamma & \text{if} \quad \text{otherwise} \end{cases} \tag{15}$$

In this case a nonrestrictive choice for Q is simple. If one has an estimate from a priori knowledge on the maximum achievable output $y_{\max}$, then clearly any individual θ_i would never be greater than $y_{\max}$. Therefore, define Q in the following equation using a safe upper bound of $\max(\theta_i) = y_{\max}$:

$$Q = \{\theta \in \mathbb{R}^n : u_{\max} - \theta_i \leq 0,\ i = 1, 2, \ldots, n\} \tag{16}$$

The convergence properties for the gradient adaptive law with parameter projection can be found in two theorems in Ref. 17, guaranteeing signal boundedness and convergence of the parameters estimates for input signals that are rich enough.

B. Thermal Model

To create a thermal control law using current as the input, we begin with two assumptions about the SMA wire actuator:

1) The length of the SMA wire is much greater than its diameter.

2) There is uniform temperature distribution along the length of the wire (neglecting any temperature deviations at the clamped ends).

With the preceding assumptions the thermal problem is reduced to the one-dimensional heat conduction-convection problem of an SMA wire. The governing equation is[3]

$$C_v(T)\frac{\partial T(x,t)}{\partial t} = k\frac{\partial^2 T(x,t)}{\partial x^2} - \frac{4h(T,D)}{D}[T(x,t) - T_\infty] + \rho_e i^2 \tag{17}$$

where $T(x,t)$ is the temperature in °C at the location x at time t, k the thermal conductivity, D the diameter of the SMA wire in m, $h(T,D)$ the coefficient of convection in W/(m²°C), C_v the specific heat in J/(m³°C), ρ_e the resistivity of the SMA wire, and i the current in amps.

By assumptions 1) and 2) the wire may be treated as being of infinite length,[3] and Eq. (17) becomes

$$C_v(T)\frac{\partial T(t)}{\partial t} = -\frac{4h(T,D)}{D}(T - T_\infty) + \rho_e i^2 \tag{18}$$

Solving Eq. (18) for $\dot{T} = \mathrm{d}T/\mathrm{d}t$ yields the equation

$$\dot{T} = -(4h/C_v D)(T - T_\infty) + (\rho_e/C_v)i^2 \tag{19}$$

The two coefficient expressions of Eq. (19) can be lumped into general parameters

$$\alpha = 4h/C_v D, \qquad \beta = \rho_e/C_v$$

and Eq. (19) takes the form

$$\dot{T} = -\alpha(T - T_\infty) + \beta u \tag{20}$$

where $u = i^2$ is the control variable. By letting $\bar{T} = T - T_\infty$, we get $\dot{\bar{T}} = \dot{T}$ because of the assumption that T_∞ is constant, and Eq. (20) assumes a classical form for model reference control (MRC), namely,

$$\dot{\bar{T}} = -\alpha \bar{T} + \beta u \tag{21}$$

For a thermal plant model of the form of Eq. (21), a standard control design[17] to force $\bar{T}$ to track a reference model of the form

$$\dot{\bar{T}}_m = -\alpha_m \bar{T}_m + \beta_m r_T \tag{22}$$

is given by the control law

$$u = -k^* \bar{T} + L^* r_T \tag{23}$$

Here r_T is a given temperature reference signal, $k^* = (\alpha_m - \alpha)/\beta$, and $L^* = \beta_m/\beta$ and α_m, β_m are the reference model parameters. For $\bar{T}$ to track r_T, we set $\alpha_m = \beta_m$. The magnitude of α_m determines the exponential rate at which $\bar{T}_m$ will approach r_T, in addition to the exponential rate at which $\bar{T}$ will approach $\bar{T}_m$ when $\bar{T}(0) \neq \bar{T}_m(0)$.

For temperature estimation let $\hat{T}$ be the estimate of the relative temperature (with respect to ambient temperature) $\bar{T}$. The KP model will then be a function of $\hat{T}$, which will be determined by integration of Eq. (21). Defining the input to the KP model in this manner allows ambient temperature, which may vary over the course of actuation, to be ignored.

C. Determination of Thermal Parameters: Calibration Procedure

The thermal model for the SMA wire of Eq. (21) is used to calculate the estimated relative temperature $\hat{T}$ of the wire. The variable $\hat{T}$ can then be used as an intermediate variable for the input to the hysteresis model to compensate for the current-rate dependence. To improve the performance for adaptive compensation using the KP model, a reasonable estimate of the thermal coefficients α and β is required. In the calibration procedure we make several assumptions that tailor the thermal model to a specific KP model representation:

1) When $y = 0$, the SMA is in the martensite phase, with a corresponding value of $\hat{T} = 0$.

2) When y equals the maximum output of the SMA actuator $y = y_{\max}$, the SMA is in the austenite phase. The corresponding temperature depends on the defined input interval for the KP model: $\hat{T}_{\max}$ is set equal to $s_{\max}$ when $y = y_{\max}$.

3) When there is no current, the SMA returns to martensite, indicated by $y \to 0$. $\hat{T}$ is assumed to approach zero as y approaches zero.

Starting with the actuator in martensitic phase, such that $y = 0$, we slowly increase the heat input $u = i^2$ to the point where y stops increasing. We denote this value of displacement as $y_{\max}$, the maximum output of the SMA actuator, and record the corresponding heat input as $u_{\max}$. The SMA is assumed to be at a steady-state temperature of $\hat{T}_{\max}$. When $\hat{T}$ attains this steady-state value, $\dot{\hat{T}} = 0$, and the parameter ratio of α/β can be solved from Eq. (21):

$$\alpha/\beta = u_{\max}/s_{\max} \tag{24}$$

Next we set the current to zero $u = i^2 = 0$ and determine the time interval Δt for y to reach a value of $0.05 y_{\max}$. With $u = 0$, Eq. (21) becomes $\dot{\hat{T}} = -\alpha \hat{T}$, for which the closed-form solution is simply $\hat{T}(t) = \hat{T}_{\max} \exp(-\alpha t)$. We can reasonably assume that when y equals 5% of $y_{\max}$ (close to full martensitic transformation), the temperature is near 5% of $\hat{T}_{\max}$, and the coefficient α can be calculated as

$$\alpha = -\frac{\ln(0.05)}{\Delta t} \tag{25}$$

The coefficient β can then be determined from the quantities α and α/β.

By determining α and β in this manner, we ensure that over the output range of the actuator $\hat{T}$ will span the input range for the hysteresis model. In addition, we will have a reasonable approximation of the temperature rate of change with respect to the heating signal $u(t) = i(t)^2$. Any discrepancies in the estimated temperature will be

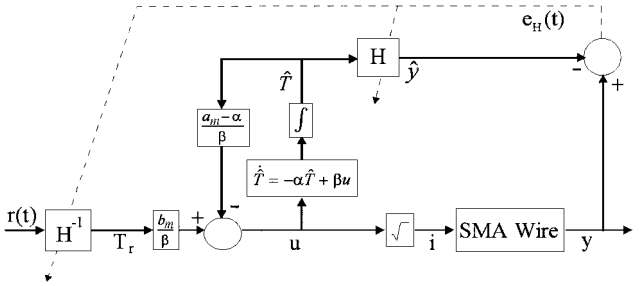

Fig. 7 Schematic of control algorithm.

accounted for by the adaptive update of the hysteresis model. In the next subsection we provide the overall control algorithm for commanding the current such that the SMA actuator tracks a desired reference displacement signal. Experimental results in Sec. IV will show that α and β need only be rough estimates, with the controller being robust over a range of values for the thermal model parameters.

D. Control Algorithm

The control algorithm used for the tracking experiments in Sec. IV can best be described by referring to the schematic in Fig. 7. A given reference displacement signal $r(t)$ is mapped into a reference temperature T_r via the hysteresis model inverse H^{-1}. Equation (23) calculates the required heating u to force $\hat{T}$ to track T_r, whereas Eq. (21) is integrated to determine $\hat{T}$. The current signal is output to the SMA wire as $i = \sqrt{u}$. Note that the current is limited by strict bounds on u, in that u is constrained to lie in the interval $[0, i_{\max}^2]$, where $i_{\max}$ is a predefined safety limit on the current. The lower limit on u essentially means that the fastest cooling that can be achieved is when the current to the SMA wire is turned off.

To adaptively update the hysteresis model to represent the y vs $\hat{T}$ relationship, the estimate of the displacement output $\hat{y}$ is generated via $H(\hat{T})$. The estimation error is calculated using the error between the actual displacement y and $\hat{y}$. The hysteresis model parameters θ_{ij} are updated using the gradient adaptive law from Sec. III.A.2, in turn updating the inverse model.

In this control methodology the thermal parameters remain constant. Although it may be possible to update the thermal parameters adaptively to represent the heating and convection more accurately for a time-varying cooling environment, in this paper the burden of accounting for these variations lies solely with the adaptive hysteresis model. Reasonable estimates of the thermal parameters serve to ensure that $\hat{T}$ remains in the defined input region of the hysteresis model. The experimental results in the next section show that the controller works even when the thermal parameters are significantly different from the calibrated values.

IV. Experimental Results in Air and Water

For all of the experiments, the KP model is defined by a discretization number of $K = 13$ resulting in 91 parameters. In previous experiments[9] KP models with up to 231 parameters have been shown to be feasible. The input region for the KP model is defined by $s_{\min} = -10$ and $s_{\max} = 60$. The KP hysteresis model is initialized with no information about the displacement vs temperature relationship at the beginning of each experiment, with the θ_{ij} set equal to $1/N = \frac{1}{91}$. The results from the following experiments show that even when there is no initial information on the hysteresis the KP model can adapt quickly to provide accurate compensation.

To examine the performance of the control strategy for a wide range of cooling environments, experiments involving the tracking of step and sinusoidal reference trajectories are conducted in air and in water. The in-air experiments use an airflow passed through a vortex cooler, parallel to the wire, to achieve faster cooling rates than in stagnant, ambient air alone. With the vortex cooler compressed air is supplied to a vortex tube and passes through nozzles that are tangent to an internal counterbore. These nozzles set the air in a vortex motion. This spinning stream of air turns 90 deg and passes down the hot tube in the form of a spinning shell. A valve at one end of the tube allows some of the warmed air to escape. What does not escape heads back down the tube as a second vortex inside the low-pressure area of the larger vortex. This inner vortex loses heat and exhausts through the other end as cold air.

Table 1 Thermal parameters from calibration for different environments

Surrounding medium	α	β
Air	0.06	1.99
Vortex cooled air	0.60	3.00
Water (0.167 m/s)	12.12	2.69
Water (0.347 m/s)	30.76	3.46

The in-water experiments use forced water convection with the flow perpendicular to the wire actuator, with flow rates of 0.167, 0.347, and 0.415 m/s. The difference in cooling between the different environments is evidenced by the calibrated thermal parameter estimates of Eq. (21), given in Table 1. Note that the thermal constants are dependent upon $s_{\max}$, the assumed maximum transformation temperature, used in Eq. (24) to calculate the ratio of α/β. For the calibrated thermal parameters given in Table 1, $s_{\max} = 60$. By looking at the relative differences between the convection-dependent term α, we can see that water flowing at 0.347 m/s has a convection rate 500 times that of stagnant air.

Although we do not use any of the material/environmental parameters from Eq. (18) to determine the values of α and β, we provide evidence that the calibrated values do indeed make sense. With values of $C_v = 3.5 \times 10^6$ J/(m^{3}C), $D = 0.00058$ m (0.023 in.), and $h = 50$ W/(m^{2}C) for a wire in air, the value of α can be calculated as

$$\alpha = \frac{4h}{C_v D} = \frac{4 \times 50}{(3.5 \times 10^6) \times 0.00058} = 0.098 \qquad (26)$$

which is in the same neighborhood as the calibrated value of $\alpha = 0.06$.

A. Forced Air-Convection Environment

The first experiment in air (with the vortex cooler) involves the tracking of a step-reference signal, with the thermal parameters being assigned the calibrated values for vortex cooled air from Table 1. The reference signal and actual displacements are shown in Fig. 8a, from which we can see that the tracking performance is excellent. The commanded current history is shown in Fig. 8b, along with the estimated temperature in Fig. 8c. Fig. 8c conveys two important pieces of information: 1) the thermal control law is effective in tracking the target temperature from $H^{-1}[r(t)]$, and 2) the temperature estimate remains within the bounds set for the KP model input.

A sinusoidal reference signal, given by Eq. (27):

$$r(t) = 0.25 + 0.15\{\sin[2\pi(f/\sqrt{10})t - \pi/2] + \cos(2\pi f t - \pi)\}\tfrac{1}{2} \qquad (27)$$

is used for the second tracking experiment in air, where f is the frequency of the sinusoid. To examine the controller performance when α and β are different from the calibrated values, the thermal parameters for this experiment are chosen to be $\alpha = 2.0$ and $\beta = 2.0$. Figure 9a shows that the displacement tracks the reference signal, with a small tracking error as shown in Fig. 9b. The frequency of the reference signal is 0.1 Hz, which is close to the maximum that can be achieved with the vortex-cooled air flow. Achieving higher frequency response from the SMA wire requires the forced water-convection environment of the water tunnel.

B. Forced Water-Convection Environment

The first experiment in the water tunnel involves tracking a step-reference signal. The flow rate of the water is 0.347 m/s, and the thermal parameters are chosen to be the calibrated values listed in Table 1. Figure 10a displays the reference and actual displacement trajectories. As with the forced air environment, there is excellent

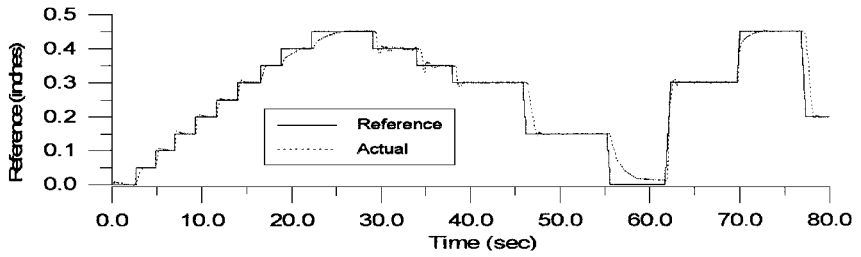

a) Reference (step) and actual

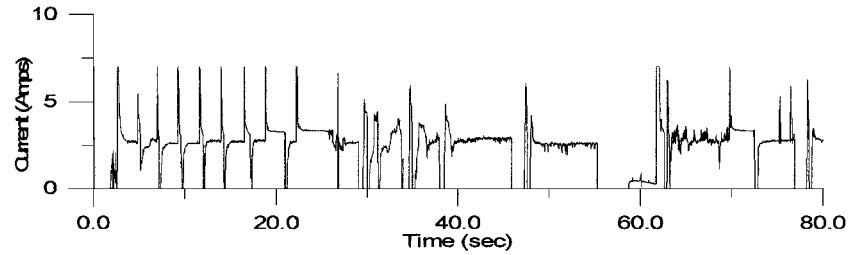

b) Commanded current

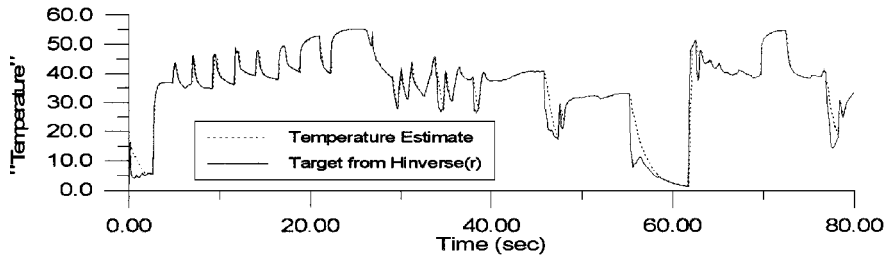

c) Target and actual "temperature"

Fig. 8 Reference signal (step) tracking. In air, vortex cooler, $\alpha = 0.6$, $\beta = 3.0$, $a_m = 20$, and $\gamma = 20$.

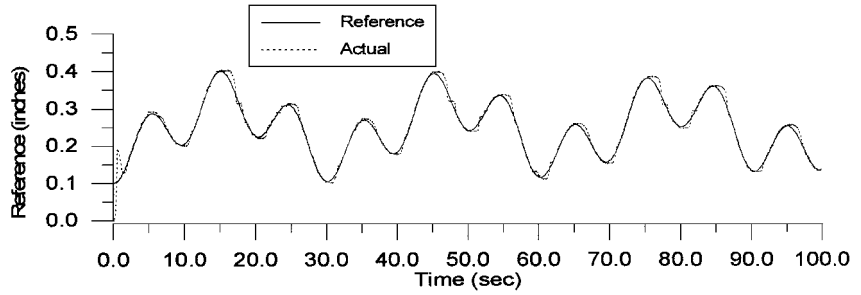

a) Reference trajectory (0.1 Hz)

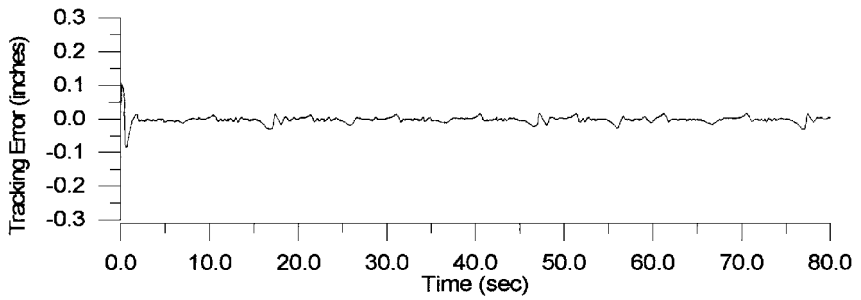

b) Tracking error

Fig. 9 Reference signal (0.1-Hz sinusoid) and tracking error. Vortex cooler, $\alpha = 2.0$, $\beta = 2.0$, $a_m = 20$, and $\gamma = 20$.

tracking of the step-reference signal. The amount of noise in the displacement measurement signal is significantly greater than that for the in-air experiment because of 1) interference from the water-tunnel motor, 2) interference from the power supply, and/or 3) physical disturbance, by the flowing water, of the string connecting the SMA wire to the lever arm. The commanded current signal in Fig. 10b can be compared with that of Fig. 8b for the forced air environment. As expected, the required current for similar deflections is much higher in the forced water environment. In addition, while the current had to be shut off to achieve the required cooling rate in air, we can see that in water a significant amount of current is still required to slow down the cooling. Figure 10c shows the estimated temperature history along with the target temperature signal from $H^{-1}[r(t)]$. Comparing Figs. 8 and 10, one can see that $\hat{T}$ is more sensitive to changes when the SMA wire is cooled using forced water rather than forced air.

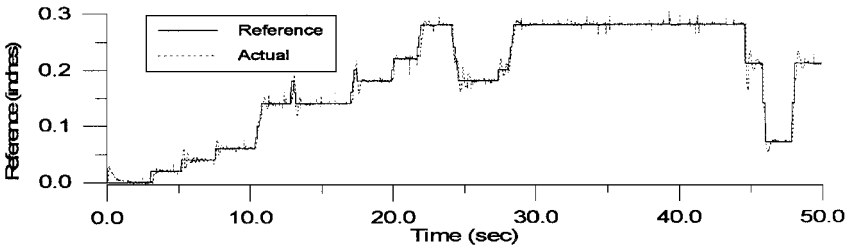

a) Reference (step) and actual

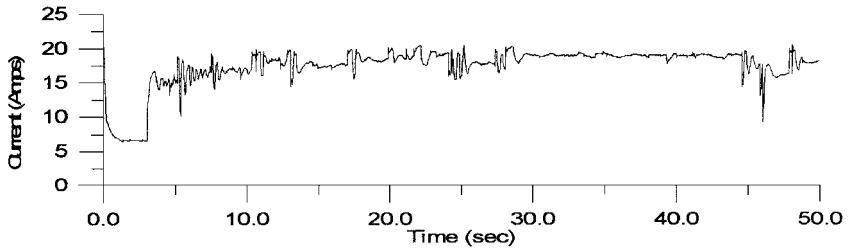

b) Commanded current

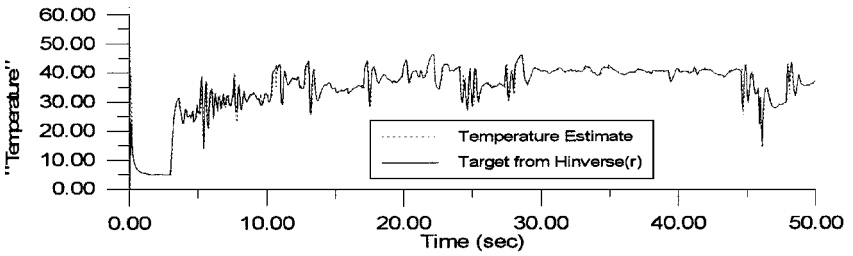

c) Target and actual "temperature"

Fig. 10 Reference signal (step) tracking. In water (0.347 m/s), $\alpha = 30.76$, $\beta = 3.46$, $a_m = 40$, and $\gamma = 20$.

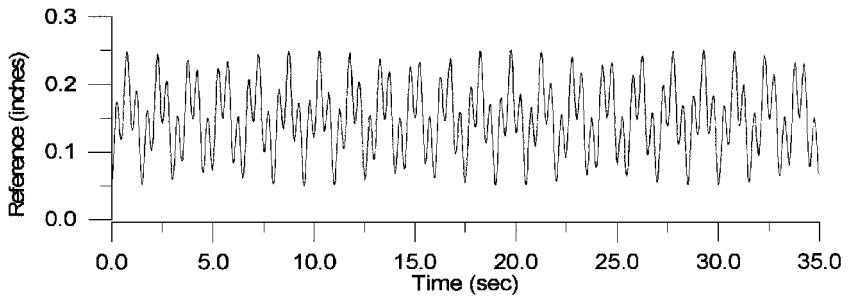

a) Reference trajectory (2 Hz)

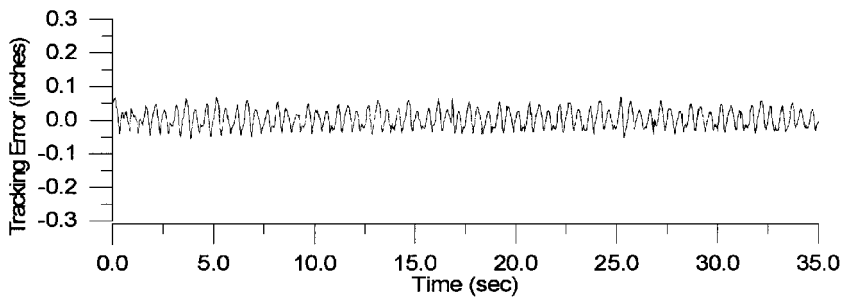

b) Tracking error

Fig. 11 Reference signal (2-Hz sinusoid) and tracking error. In water (0.415 m/s), $\alpha = 30.76$, $\beta = 3.46$, $a_m = 80$, and $\gamma = 20$.

The next two experiments involve tracking a sinusoid, similar in form to that of Eq. (27), but with higher frequencies. The water flow rate is 0.415 m/s to achieve faster cooling; however, the thermal parameters remain at the values of the 0.347-m/s calibration. Figure 11a shows the 2-Hz sinusoidal reference signal over 35 s of actuation, with the tracking error shown in Fig. 11b. The sinusoidal nature of the tracking error is caused by a phase lag in the tracking, seen in the enlarged plot for a 5-s interval in Fig. 12a We can see that, except for the phase lag, the displacement signal follows the characteristics of the reference signal. The current signal for the 5-s interval, shown in Fig. 12b shows repeatable current cycles at a 2-Hz frequency. Again, we show the estimated temperature history in Fig. 12c. Using the estimated temperature, the displacement-vs-temperature hysteresis is depicted in Fig. 13. The major and minor loops are representative of the form of hysteresis between displacement and actual temperature[10] and can easily be captured by the KP model.

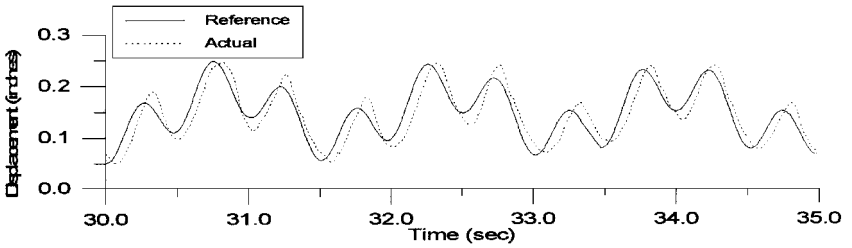

a) Reference trajectory (2 Hz) and actual, 5-s interval

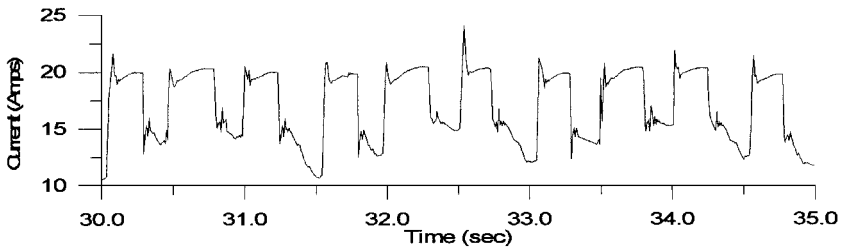

b) Commanded current over 5-s interval

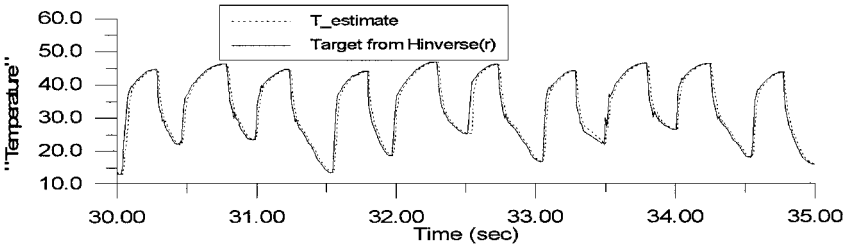

c) Target and actual "temperature"

Fig. 12 Reference signal (2-Hz sinusoid) and commanded current. In water (0.415 m/s), $\alpha = 30.76$, $\beta = 3.46$, $a_m = 80$, and $\gamma = 20$.

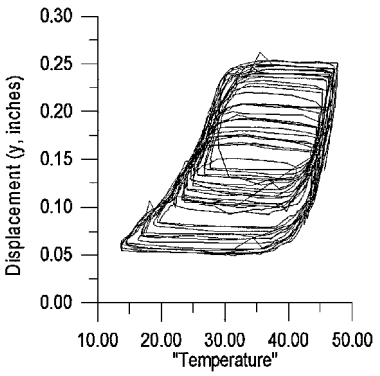

Fig. 13 Hysteresis between displacement and temperature. Reference signal (2-Hz sinusoid). In water (0.415 m/s), $\alpha = 30.76$, $\beta = 3.46$, $a_m = 80$, and $\gamma = 20$.

One factor that contributed to the phase lag is the ramp-up time for the power supply. A rise time of 0.054 s to go from 0 to 20 A becomes significant for an actuation frequency of 2 Hz (10% of the period). Another limitation to achieving higher frequency control is the data sampling rate—about 100 Hz for the Pentium 133. It is reasonable to assume that a faster sampling rate, improved power supply, and/or incorporating knowledge of the lag in the thermal controller will significantly improve the tracking performance at higher frequencies. In future work we will address the issues of lag compensation and sampling rate to achieve tracking control for signals above 10 Hz.

V. Conclusions

We have provided a control methodology that uses a rough estimate for the thermal properties of an SMA wire actuator and its interaction with the surrounding medium in order to estimate the temperature. The temperature estimate can then be used when actual temperature measurements are unavailable, in conjunction with an adaptive hysteresis model for compensation. Experiments in air and in water have shown that the control methodology provides for excellent tracking of both step and sinusoidal reference trajectories over a broad range of thermal environments. For biomimetic applications that use the cooling properties of water, we have shown that we can achieve actuation control of an SMA wire at frequencies up to 2 Hz. In the future, we expect that by compensating for the lag in the power supply and increasing the sampling rate, the tracking performance of the proposed adaptive controller will significantly improve. We will also investigate the use of an electrically insulative fluid, such as glycol, that circulates through a channel around the SMA wire in a closed system.

Acknowledgments

This work was supported by the Office of Naval Research and Aeroprobe, Inc., through the STTR program under Contract N00014-98-C-0061. The authors would like to thank the technical monitor of the project, Teresa McMullen, for her support. Special thanks also go to Richard Allen for his help with the experimental setup.

References

[1]Tanaka, K., "A Thermomechanical Sketch of Shape Memory Effect: One-Dimensional Tensile Behavior," *Res Mechanica*, Vol. 18, No. 3, 1986, pp. 251–263.

[2]Giurgiutiu, V., Chaudry, Z., and Rogers, C., "Active Control of Helicopter Roter Blades with Induced Strain Actuators," AIAA Paper 94-1765, 1994, pp. 288–297.

[3]Shu, S., Lagoudas, D., Hughes, D., and Wen, J. T., "Modeling of a Flexible Beam Actuated by Shape Memory Alloy Wires," *Smart Material Structures*, Vol. 6, No. 3, 1997, pp. 265–277.

[4]Chaudry, Z., and Rogers, C., "Bending and Shape Control of Beams Using SMA Actuators," *Journal of Intelligent Material Systems and Structures*, Vol. 2, No. 4, 1991, pp. 581–602.

[5]Kurdila, A. J., and Webb, G. V., "Compensation for Classes of Distributed Hysteresis Operators and Representation of Active Structural Systems," *Journal of Guidance, Control, and Dynamics*, Vol. 20, No. 6, 1997, pp. 1133–1140.

[6]Hughes D., and Wen, J., "Preisach Modeling and Compensation for Smart Material Hysteresis," *SPIE Active Materials and Smart Structures*, Vol. 2427, 1994, pp. 50–64.

[7]Dickinson, C. A., and Wen, J. T., "Feedback Control Using Shape Memory Alloy Actuators," *Journal of Intelligent Material Systems and Structures*, Vol. 9, No. 4, 1998, p. 242.

[8]vander Wijst, M., "Shape Control of Structures and Materials with Shape Memory Alloys," Ph.D. Dissertation, Technishe Univ. Eindhoven, 1998.

[9]Webb, G., "Adaptive Identification and Compensation for a Class of Hysteresis Operators," Ph.D. Dissertation, Dept. of Aerospace Engineering, Texas A&M Univ., College Station, TX, May 1998.

[10]Webb, G. V., Kurdila, A. J., and Lagoudas, D. C., "Hysteresis Modeling of SMA Actuators for Control Applications," *Journal of Intelligent Material Systems and Structures*, Vol. 9, No. 6, 1998, pp. 432–448.

[11]Visintin, A., *Differential Models of Hysteresis*, Springer–Verlag, New York, 1994, pp. 1, 2, 97–129.

[12]Preisach, F., "Uber die Magnetische Nachwirkung," *Zeitschrift fur Physik*, Vol. 94, Nos. 5, 6, 1935, pp. 277–302.

[13]Mayergoyz, I., *Mathematical Models of Hysteresis*, Springer–Verlag, New York, 1991, pp. 1–63.

[14]Krasnoselskii, M., and Pokrovskii, A., *Systems with Hysteresis*, Nauka, Moscow, 1983.

[15]Banks, H., Kurdila, A., and Webb, G., "Identification of Hysteretic Control Influence Operators Representing Smart Actuators: Formulation," Center for Research in Scientific Computation, North Carolina State Univ., TR CRSC-TR96-14, Raleigh, NC, April 1996.

[16]Banks, H., Kurdila, A., and Webb, G., "Modeling and Identification of Hysteresis in Active Material Actuators, Part (ii): Convergent Approximations," *Journal of Intelligent Material Systems and Structures*, Vol. 8, No. 6, 1997, pp. 536–550.

[17]Ioannou, P., and Sun, J., *Robust Adaptive Control*, Prentice–Hall, Upper Saddle River, NJ, 1996, pp. 180–186, 203–206.

A. Chattopadhyay
Associate Editor